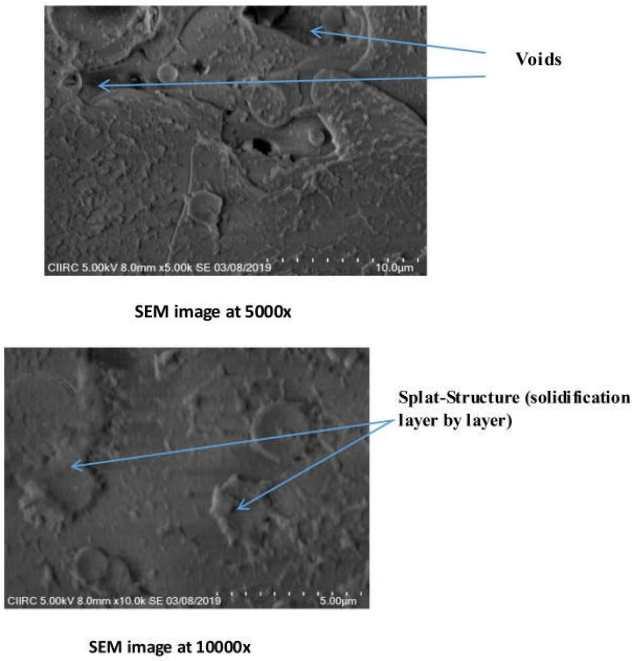

Figure 5: SEM images shows the splat morphology of the coating and a network of pores, cracks and voids, unmelted particles

Energy Dispersive Spectroscopy (EDS) Studies

Figure 6 below shows the EDS spectrum for the coated specimen and Table 3 shows the quantitative results.

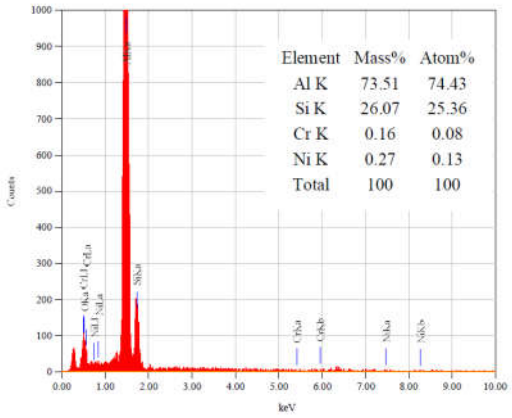

Figure 6: EDS plot of the coated specimen

Table 3: EDS Quantitative results

Element Line	Weight %	Weight % Error	Atom %	Atom % Error
O K	34.34	± 0.82	47.50	± 1.13
Al K	49.95	± 1.14	40.97	± 0.93
Si K	13.36	± 0.81	10.53	± 0.64
Si L	---	---	---	---
Cr K	2.35	± 2.35	1.00	± 1.00
Cr L	---	---	---	---
Fe K	---	---	---	---
Fe L	0.00	---	0.00	± 0.00
Ni K	---	---	---	---
Ni L	0.00	---	0.00	± 0.00
Total	100.00		100.00	

The EDS plots reveal the presence of the elements- Aluminium, Silicon, Oxygen, and traces of Nickel, and Chromium with a higher weight percentage of aluminium, silicon and oxygen due to these elements present in the ceramic top coat. The presence of the bond coat material may be due to a higher network of porosity and voids of the top coat at some local zones.

Coating Thickness Results

Table 4 below shows readings taken at 10 different location's on the coated surface for the measurement of coating thickness.

Average thickness of the coating consisting of the bond coat and the top coat on mild-steel is 283.5µm. A lower thickness is desired to improve the adhesion of the coating on the substrate. Thermal spraying using HVOF technique provides thickness in the above range, which is acceptable for many applications.

Table 4: Coating Thickness measurements

Trial No.	Coating Thickness (µm)	Trial No.	Coating Thickness (µm)
1	252	6	296
2	260	7	271
3	270	8	294
4	269	9	316
5	258	10	349
		Average	283.5

Surface Roughness Results

The surface roughness measurements are shown for the bare sand blasted MS specimens and the ceramic coated specimens in the Table 5 below.

Surface roughness of mild steel samples is shown in the table, which is required for the coating adhesion to take place. The roughness is more in the ceramic coated layer due to the layered formation of splats during spraying. A buffing operation if required can be carried out to improve the surface finish.

Table 5: Surface Roughness: Ra-Average Ratio, Rq-Root Mean Square, Rz-Average distance between highest peak and lowest valley

Materials	Ra(µM)	Rq(µm)	Rz(µm)
Sand Blasted MS	3.153	3.845	14.771
Ceramic Coated MS	5.475	6.671	26.946

Corrosion Rate Results

Tafel plots and the results are shown below for the sea water base. The I_{corr} value of 0.1338116 mA/cm² for sea water base and corrosion rate of 1.55 mm/year were measured for the coated samples. Tafel plots and corrosion rate of stainless steel and MS have been studied for comparison. Tafel plots of the AISI 316 stainless steel and AISI 1010 carbon steel showed an Icorr measurement of -4 mA/cm2 and -2 mA/cm2 respectively as per literature [23]. The electrolyte consisted of 3.0 wt% solution of chloride ions and the test was conducted at a temperature of 24˚C ± 1.0˚C; scan rate of 0.5 mV·s−1.This implies a low corrosion rate for SS 316 and Carbon steel 1010. Refer to Figure 7 for the tafel plots.

I_{corr} values (ranging from 8 to 50 mA/cm²)and corrosion rates (ranging from 0.904 to 5.921 mm/year are much higher in the case of bare MS specimens tested in sea water as per literature [24].Figure 8 shows the tafel plot for sea water base and table 6 shows the measured values of the

process parameters. Figure 9 shows the test specimen before and after polarization test.

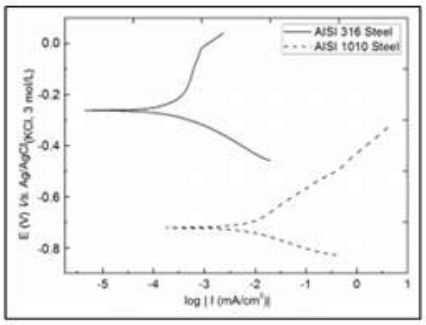

Stainless Steel Tafel plot

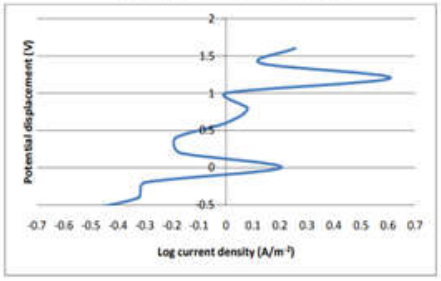

Tafel plot for Mild Steel(Sea Water Base)

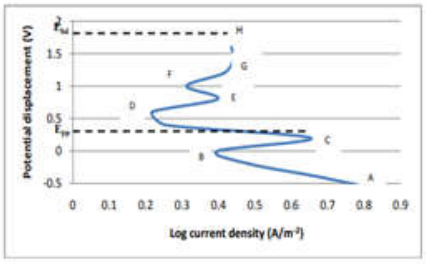

Tafel plot for Mild Steel (Synthetic Water Base)

Figure 7: Tafel plot for SS and MS

Table 6: Corrosion rate results of coated specimens in sea water base

Test type	Cyclic sweep
Area (cm^2)	1
Rest Potential (mV)	-563.62
Metal	Mild Steel
Metal factor	1163
LPR ($Ohm.cm^2$)	207.8
Ba (mV)	80.254
Bc (mV)	314.92
Icorr (mA/cm^2)	0.1338116
Corrosion Rate (mm/year)	1.5562
Corrosion rate (mils/yr)	61.268
Intercept (mA/cm^2)	0
Intercept corrosion rate (mm/year)	0
Intercept corrosion rate (mils/yr)	0
IR Compensation value ($Ohm.cm^2$)	N/A
Start Potential	-300 mV
Reverse Potential	700 mV
Sweep Rate	2.778 mV/min
Cycles	1.5
Readings Per Test	Automatic
Cell Settle Time	5 seconds
Limit at	400 mA/cm^2

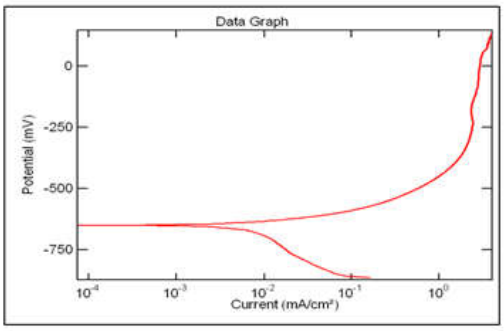

Tafel Plot for sea water

Figure 8: Tafel Plot for coated specimens

Test sample before polarization test

Test sample after polarization test

Figure 9: Test specimen before and after polarization test

It is apparent that corrosion rate is satisfactory and good enough for commercial applications. The result obtained is similar to that of stainless steel. But for advanced ceramics, a lower corrosion rate is desired. The reasons for a high corrosion rate generally are due to a high percentage of porosity, cracks, voids and oxidation networks. Porosity in HVOF sprayed coatings are generally of the order of 6 to 21 % by volume. Better process control and use of vacuum or use of inert shroud gas may be adopted to reduce the porosity levels. A denser coating can be achieved and enhanced corrosion rates can be ensured as denseness (impermeability) plays a major role in the corrosion resistance of coatings.

Conclusions

Ceramic Coating was carried out on Mild Steel using HVOF technique. Characterization studies like XRD, SEM, EDS, Coating thickness, Surface Roughness, coating adhesion and polarization test for corrosion were conducted. The XRD results showed the different phases present in the coating. The SEM and EDS techniques make it possible to identify and determine the microstructure and composition

of the coated surface. The corrosion rate of 1.5562 mm/yr was obtained in the Polarization test. The coated material is comparable to bulk SS and Nickel. This is an acceptable corrosion rate where we can use this for many marine applications. By taking the above shown results into consideration ceramic coatings can be done on mild-steel for extreme environmental applications. At the same time with better process control, and with the use of inert shroud gas or vacuum, the coating can be made denser resulting in an improved morphology devoid of defects like high porosity, voids and unmelted particles. This can enhance the life of the coating for many applications. Hence the future scope of the work will cover these aspects to make the coating denser and with fewer defects.

Declaration of interest statement

There is no conflict of interest in this work. This is the research work done by the author in his Institute.

References

1. Basu, S.N., Structure and properties of functionally graded environmental barrier coatings for ceramic components in gas turbines, International conference on advanced materials and composites (ICAMC-2007), Oct 24-26, organized by National Institute for interdisciplinary science and technology, CSIR, Trivandrum, 2007.
2. Juliana Anggono, Mullite Ceramics: Its Properties, Structure, and Synthesis, Jurnal Teknik Mesin, 2005, 7(2), 1-10.
3. B. Viswanath, S. Vijayarangan, Characterization studies of mullite coatings on cast aluminum, J. Therm. Spray Technol., 2011, 21 (2), 325-334.
4. M. BillahBhatty, F. Ahmad Khalid, and A. Nusair Khan, Behavior of Calcia-Stabilized Zirconia Coating at High Temperature, Deposited by Air Plasma Spraying System, J. Therm. Spray Technol., 2012, 21(1), 121-131.
5. D. J. Branagan, M. Breitsameter, B. E. Meacham, V.Belashchenko, High-Performance Nanoscale Composite Coatings for Boiler Applications, J. Therm. Spray Technol., 2005, 14 (2), 196-204.
6. G. I. Cubillos, J. J. Olaya, M. Bethencourt, G. Cifredo, and G. Blanco, Resistance to Corrosion of Zirconia Coatings Deposited by Spray Pyrolysis in Nitrided Steel, J. Therm. Spray Technol., 2013, 22(7), 1242-1252.
7. D. Fantozzi, V. Matikainen, M. Uusitalo, H. Koivuluoto, P. Vuoristo, Effect of Carbide Dissolution on Chlorine Induced High Temperature Corrosion of HVOF and HVAF Sprayed Cr3C2-NiCrMoNb Coatings, J. Therm. Spray Technol., 2018, 27, 220–231.
8. Hitesh Vasudev, Lalit Thakur, Amit Bansal, Harmeet Singh, Sunny Zafar, High temperature oxidation and erosion behaviour of HVOF sprayed bi-layer Alloy-718/NiCrAlY coating, Surf. Coat. Technol., 2019, 362, 366-380.
9. T. Hussain, D. G. McCartney, P. H. Shipway, T. Marrocco, Corrosion Behavior of Cold Sprayed Titanium Coatings and Free Standing Deposits, J. Therm. Spray Technol., 2011, 20(1-2), 260- 274.
10. Chen Jiang, Eric H. Jordan, Alan B. Harris, Maurice Gell, and Jeffrey Roth, Double-Layer Gadolinium Zirconate/Yttria-Stabilized Zirconia Thermal Barrier Coatings, Deposited by the Solution Precursor Plasma Spray Process, J. Therm. Spray Technol., 2015, 24(6), 895-906.
11. Anup Kumar Keshri and Arvind Agarwal, Wear Behavior of Plasma-Sprayed Carbon Nanotube-Reinforced Aluminum Oxide Coating in Marine and High-Temperature Environments, J. Therm. Spray Technol., 2011, 20(6), 1217-1230.
12. Heli Koivuluoto, JonneNa¨kki, and Petri Vuoristo, Corrosion Properties of Cold-Sprayed Tantalum Coatings, J. Therm. Spray Technol., 2009, 18(1), 75 – 82.
13. S. Paul, B. Syrek-Gerstenkorn, Can Thermally Sprayed Aluminum (TSA) Mitigate Corrosion of Carbon Steel in Carbon Capture and Storage (CCS) Environments, J. Therm. Spray Technol., 2017, 26, p 184-194.
14. J. H. Perepezko, T. A. Sossaman, M. Taylor, Environmentally Resistant Mo-Si-B-Based Coatings, J. Therm. Spray Technol., 2017, 26, 929–940.
15. SekarSaladi, Jyoti V Menghani, Satya Prakash, Characterization and Evaluation of Cyclic Hot Corrosion Resistance of Detonation-Gun Sprayed Ni-5Al Coatings on Inconel, J. Therm. Spray Technol., 2015, 24(5), 778-788.
16. T.S.Sidhu, A. Malik, S. Prakash, and R.D. Agrawal, Oxidation and Hot Corrosion Resistance of HVOF WC-NiCrFeSiB Coating on Ni- and Fe-based Super alloys at 800^{0}C, J. Therm. Spray Technol., 2007, 16(5-6), 844-849.
17. S Shrestha, A J Sturgeon, The use of advanced thermal spray processes for corrosion protection in marine environments, Surface Engineering, 2004, 20(4),237-243.
18. Y. Wang, Y.G. Zheng, W. Kea, W.H. Sun , W.L. Hou , X.C. Chang, J.Q. Wang, Slurry erosion–corrosion behaviour of high-velocity oxy-fuel (HVOF) sprayed Fe-based amorphous metallic coatings for marine pump in sand-containing NaCl solutions, Corrosion Science, 2001, 53, 3177–3185.
19. S. Vignesh , K. Shanmugam , V. Balasubramanian , K. Sridhar, Identifying the optimal HVOF spray parameters to attain minimum porosity and maximum hardness in iron based amorphous metallic coatings, Defence Technology, 2017, 13, 101-110.
20. Jin Kawakita, Seiji Kuroda, Takeshi Fukushima, Toshiaki Kodama, Development of dense corrosion resistant coatings by an improved HVOF spraying process, Science and Technology of Advanced Materials, 2003, 4, 281–289.
21. Richard Piolaa, Andrew S. M. Angb, Matthew Leighc, Scott A. Wadeb, A comparison of the antifouling performance of air plasma spray (APS) ceramic and high velocity oxygen fuel (HVOF) coatings for use in marine hydraulic applications, Biofouling, 2018, 34(5), 479–491.
22. https://www.mee-inc.com/hamm/electrochemical-corrosion-testing/Electrochemical Corrosion Testing.
23. Roberta R. Moreira, Thiago F. Soares, Josimar Ribeiro, Electrochemical Investigation of Corrosion on AISI 316 Stainless Steel and AISI 1010 Carbon Steel: Study of the Behavior of Imidazole and Benzimidazole as Corrosion Inhibitors, Adv. Chem. Engineer. Sci., 2014, 4, 503-514.
24. O. I. Sekunowo, S. O. Adeosun, G. I. Lawal, Potentiostatic polarization responses of mild steel in seawater and acid environments, IJSTR, 2013, 2(10),139-145.